

## On the back-firing instability

M. Argentina

*Division of Engineering and Applied Sciences, Harvard University, Cambridge, Massachusetts 02139*

O. Rudzick

*Abteilung Physikalische Chemie, Fritz-Haber-Institut der Max-Planck-Gesellschaft, Faradayweg 4-6, 14195 Berlin, Germany*

M. G. Velarde<sup>a)</sup>

*Instituto Pluridisciplinar, Paseo Juan XXIII, n. 1, 28040 Madrid, Spain*

(Received 19 January 2004; accepted 25 June 2004; published online 16 September 2004)

The onset of the back-firing instability is studied in a one-dimensional spatially extended and dissipative system, where propagating localized solutions become unstable. It corresponds to the emission in the tail of a solitary wave of a new wave propagating in the opposite direction. The transition is illustrated, in geometrical terms, using a model normal form equation. © 2004 American Institute of Physics. [DOI: 10.1063/1.1784911]

**In spatially extended dynamical systems, the transition from complex behavior to ordered state may be understood in terms of synchronization. Here we focus attention on the particular case of synchronization of oscillations in a one-dimensional spatially extended system when an external resonant signal is injected. An example is an array of lasers submitted to an external electric field whose frequency is close to the self-oscillation of the units. Thus, we investigate the evolution of a nonlinear oscillatory medium submitted to a resonant signal. In the model equation describing the onset of the 1:1 parametric resonance, the back-firing instability is observed. This instability appears when a localized propagating pulse becomes unstable and splits into two new counterpropagating solutions that upon an eventual collision disappear due to dissipation.**

### I. INTRODUCTION

The popular paradigm used to study complex dynamics including the transition to spatio-temporal chaos is the complex Ginzburg–Landau equation (CGLE), although other avenues have been suggested.<sup>1–4</sup> Here, we investigate the evolution of a nonlinear oscillatory medium submitted to a resonant signal where the back-firing instability is observed.<sup>5</sup> It is an instability that appears when a localized propagating pulse becomes unstable and splits into two new counterpropagating structures that, upon collision, disappear presumably due to dissipation.<sup>6</sup>

The successive processes of splitting and annihilation of the pulses generate a spatiotemporal diagram that looks like a Sierpinski gasket,<sup>7</sup> as seen in Fig. 1. Asymptotically, for long time intervals, the spatiotemporal evolution appears to be complex, and this can be understood<sup>5</sup> from the perspective of spatiotemporal intermittency.<sup>8</sup> This analogy with intermittency rests on the idea that the localized structures and

their interactions are at the origin of the complexity shown in Fig. 1 with wide regions where the evolution is simple (laminar). In the context of the CGLE, similar evolutions have been observed in the regime of defect-chaos turbulence.<sup>9</sup> Our aim is to show that the back-firing instability is a robust mechanism generating spatiotemporal complexity and, possibly, chaos. This genericity is found in various systems. For example, in a model of CO oxidation on Pt(110) surfaces this phenomenon has been studied,<sup>10</sup> or in models of autocatalytic chemical reactions,<sup>6,11</sup> in nonlinear optics,<sup>12</sup> presumably it occurs in the process of pigmentation observed on sea-shells,<sup>13</sup> in neurodynamics models like in the Morris–Lecar model,<sup>14,15</sup> and in fluid-drag experiments.<sup>16</sup> Also when discussing the dynamics of holes and defects in the one-dimensional CGLE, the back-firing-like instability has been advocated.<sup>2,3,10</sup>

As no geometrical arguments providing a qualitative understanding of the back-firing instability have yet been proposed, we provide here such a geometrical description of the instability and criteria for its onset.

### II. NORMAL FORM AND ARNOLD TONGUE

Let us consider the spatiotemporal dynamics of a one-dimensional spatially extended oscillating medium subject to an external oscillatory signal. Let us focus attention on the 1:1 parametric resonance using the following normal form equation:<sup>17,18</sup>

$$A_t = (1 + i\nu)A - (1 + i\alpha)|A|^2A + (1 + i\beta)A_{xx} + B. \quad (1)$$

Equation (1) describes the evolution of the complex amplitude  $A$  of the oscillations of the medium, in the reference frame of the external forcing signal whose amplitude is  $B$ . The variables  $t$  and  $x$  stand for time and space, respectively. The quantity  $(\nu - \alpha)$  measures the detuning between the (nonlinear) frequency of the medium and the frequency of the injected signal at threshold. The parameter  $\beta$  accounts for the dispersion of the medium. System (1) exhibits various spatiotemporal behaviors, including forms of spatiotemporal

<sup>a)</sup>Electronic mail: velarde@fluidos.pluri.ucm.es

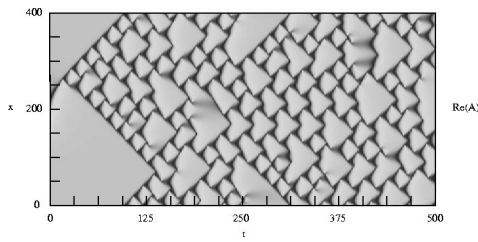


FIG. 1. Spatiotemporal diagram of the real part of  $A$  in Eq. (1). Parameter values:  $\alpha=2$ ,  $\nu=2$ , and  $\beta=0$ . Time is running left to right.

intermittency.<sup>1,18</sup> Since Eq. (1) is written in the reference frame of the external signal, stationary solutions are locked with the frequency of the forcing. Let  $A_L$  be the stationary (in time) and homogeneous (in space) state of Eq. (1). The white region of the parameter space of Fig. 2, limited by the curve  $B=B_T(\nu, \alpha)$ , is the so-called Arnold tongue.<sup>19</sup> It is inside this domain, that system (1) has the fixed point  $A_L$  as stable solution. Outside of this region,  $B < B_T(\nu, \alpha)$ , no more phase locked solutions exist and the medium is oscillating at a frequency that differs from the external signal. In order to analyze the back-firing instability, we shall consider the region where the value of  $B$  is small and near the resonance, i.e.,  $(\nu - \alpha)$  is small.<sup>5</sup>

### III. PHASE KINKS AND NUCLEATION SOLUTIONS

Let us search for nonhomogeneous solutions of Eq. (1). Inside the Arnold tongue,  $B > B_T(\nu, \alpha)$ , and for low enough values of the parameter  $B$ , nonhomogeneous propagating solutions have been observed in the numerical simulations.<sup>5,20</sup> These structures connect asymptotically in space the stable rest state  $A_L$ . In fact, one can interpret these propagating entities as to  $2\pi$ -phase kinks by observing the behavior of the phase of the complex field  $A$  of the pulse, as shown in Fig. 3(a). Due to its unsteadiness, the pulse represents a displacement of a local unlocked region.

Localized propagating structures, like phase kinks, are found by searching for solutions of Eq. (1) in the moving frame,  $\xi = x - Vt$ , where  $V$  is the velocity of the phase kink. This change of variables allows us to reduce the partial dif-

ferential equation (1) to an ordinary differential equation (ODE). In this (ODE) dynamical system, the phase kink is a homoclinic orbit of the fixed point,  $A_L$ , when  $\xi \rightarrow \pm\infty$ . It exists provided the unstable manifold of  $A_L$  intersects tangentially the stable manifold of  $A_L$ .<sup>21</sup> Counting arguments allow one to provide the necessary conditions for obtaining the tangential intersection.<sup>1</sup> In our system, the connection is never satisfied except if one free parameter is suitably adjusted. The free parameter here is the velocity,  $V$ , of the phase kink. This is a classical mechanism for velocity selection for moving interfaces in nonvariational systems.<sup>21</sup> Since we want to solve a boundary value problem, computing the velocity is not a straightforward task. We opt to use the continuation software AUTO97<sup>22</sup> and use as an initial guess a phase kink and its estimated velocity obtained in the numerical simulation of Eq. (1).

Figure 3(a) shows such a spatial profile of a phase kink. We have also done a numerical continuation of the phase kink solutions in the parameter space. Given  $\alpha$  and  $\nu$ , the control parameter,  $B$ , is varied and the corresponding velocity,  $V$ , is found. Our numerical computations show that phase kinks exist only for a limited range of values of  $B$ . A necessary condition for the existence of a phase kink is the presence of the stable fixed point,  $A_L$ , in system (1). This is why the domain of existence starts exactly at the edge of the Arnold tongue and  $B > B_T(\nu, \alpha)$ . By increasing the value of the parameter,  $B$ , a fold [Fig. 3(b)] occurs at  $B = B_{SN}(\nu, \alpha)$ . Accordingly, the interval providing the existence of the phase kink is  $B_T(\nu, \alpha) < B < B_{SN}(\nu, \alpha)$ . Due to the presence of the fold at  $B = B_{SN}(\nu, \alpha)$ , two values of the velocity,  $V$ , are found in this interval, hence the coexistence of two phase kinks. At  $B = B_{SN}(\nu, \alpha)$  we have a saddle-node bifurcation, where both phase kinks disappear. The linear stability analysis of the two pulses has been assessed numerically with a pseudo-spectral technique, using 500 modes. As expected, inside the Arnold tongue and when  $B < B_{SN}(\nu, \alpha)$ , system (1) has a stable phase kink (denoted  $\phi_-$ ), and an unstable one (denoted  $\phi_+$ ); both disappear at the saddle-node bifurcation point,  $B = B_{SN}(\nu, \alpha)$ .

Inside the interval  $B_T(\nu, \alpha) < B < B_{SN}(\nu, \alpha)$ , we know

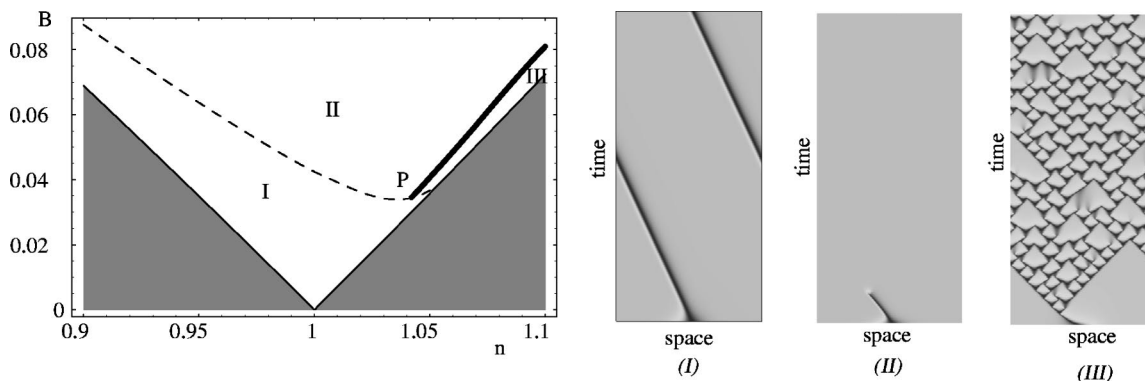


FIG. 2. Phase diagram of Eq. (1) obtained for  $\beta=0$  and  $\alpha=1$ . The white region represents the Arnold tongue. Region I: Bistability between phase kinks and the locked state,  $A_L$ . Region II: Stable locked state. Region III: Bistability between the locked state,  $A_L$ , and the back-firing regime (see Fig. 1). The dashed curve corresponds to the saddle-node bifurcation of the pulses,  $B = B_{SN}(\nu, \alpha)$ , and the thick solid line at the borders of the Arnold tongue is  $B = B_T(\nu, \alpha)$ . The three typical spatiotemporal diagrams of the real part of  $A$ , in domain with size 400, recorded over 1600 units of time, are also shown. Time proceeds as we move up (vertical axis) in the figures.

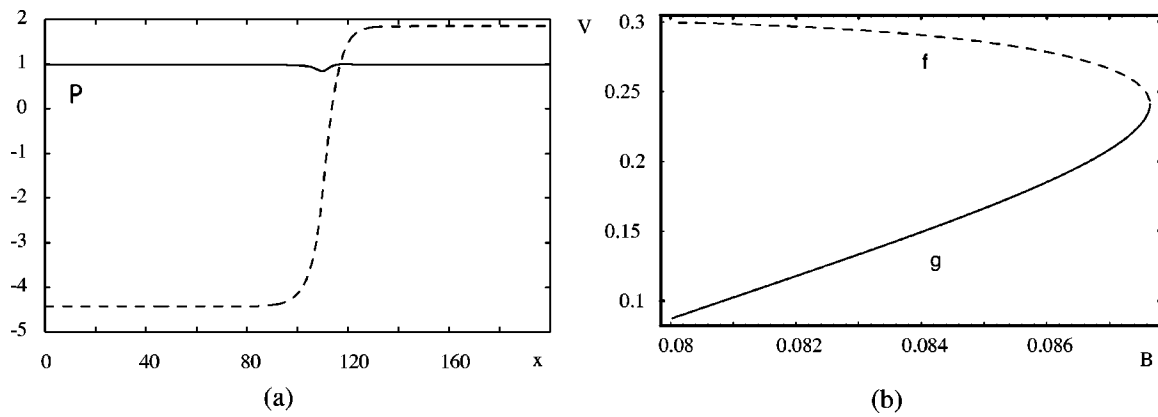


FIG. 3. (a) Profile of a phase kink obtained for the parameter values:  $\nu=0.9$ ,  $\alpha=1$ ,  $B=0.08$ ,  $\beta=0$ , and  $V=0.087$ . The solid (respectively, dashed) line accounts for the amplitude (respectively, phase) of the solution. (b) Velocity of the phase kink as a function of the parameter  $B$ . The solid (respectively, dashed) line depicts the stable (respectively, unstable) branch.

two stable solutions  $A_L$  and  $\phi_-$ . In order to create stable phase kinks, starting from the stable rest state  $A_L$ , a finite perturbation must be applied to the system. For low enough perturbation amplitudes, the system relaxes to its rest state, while for high perturbation levels, propagating pulses are created. Accordingly, there is a barrier separating the two attractors. Such a separatrix may be provided by the codimension-one stable manifold of a stationary solution.<sup>23–25</sup> We have found numerically a stationary solution  $\Gamma(x)$  in Eq. (1). Numerical linear stability analysis shows that the spectrum of  $\Gamma(x)$  has only one eigenvalue with positive real part. Hence the stable manifold of  $\Gamma(x)$ , which we call  $\mathcal{W}_s(\Gamma)$ , has codimension one, and acts like a separatrix, as it splits the phase portrait into two regions. One region has the rest state  $A_L$  as an attractor, and the other has the flow describing the propagation of two counterpropagating kinks.  $\Gamma$  is like a nucleation solution, and  $\mathcal{W}_s(\Gamma)$  acts as the nucleation manifold. The nucleation solutions are also called scatters<sup>26</sup> or homoclons.<sup>27</sup>

#### IV. THREE SPATIOTEMPORAL REGIMES

Let us now discuss the various spatiotemporal regimes that have been observed inside the Arnold tongue. The dispersive effects (measured by  $\beta$ ) may be very complex. For example, when no forcing exists, i.e.,  $B=0$ , when  $1+\alpha\beta$  becomes negative, homogeneous oscillations become unstable and the medium exhibits phase turbulence, defect turbulence or spatiotemporal intermittency.<sup>1,21,28</sup> The external forcing may re-synchronize the system when the forcing amplitude becomes high enough.<sup>18</sup> Here, we restrict consideration to the case  $\beta=0$  and hence the spatial coupling in the medium is taken purely diffusive.

We have investigated the phase diagram of Eq. (1) by integrating it numerically. The numerical schemes for time integration were either a fourth-order Runge–Kutta method or either a second-order Adams–Bashforth (Crank–Nicolson) method. The space derivatives have been computed numerically with a central difference-scheme at second- or fourth-order precision. Time step is  $5 \times 10^{-2}$  and space step is 0.2.

Figure 2 illustrates the three different spatiotemporal behaviors observed inside the Arnold tongue. In region I, bistability between the homogeneous solution and stable propagating phase kinks; in region II, the attractor is the locked state  $A_L$ ; in region III, bistability between a complex spatiotemporal behavior and the spatially homogeneous state  $A_L$ .

Thus in the spatiotemporal diagram (III) of Fig. 2 we can see that the phase kink propagates for a short time interval and then disappears yielding to a spatiotemporal defect. The appearance of the defect is necessary, since a  $2\pi$ -phase jump is removed in the complex field. After the creation of the defect, the residual product grows and produces two new kinks. This residual might be considered as a localized perturbation of the homogeneous stable state,  $A_L$ . If it becomes big enough it brings the flow over the stable manifold,  $\mathcal{W}_s(\Gamma)$ , of the nucleation solution,  $\Gamma$ , and hence creates two new phase kinks. Since  $\Gamma$  is symmetric in the space variable, due to the symmetry  $x \rightarrow -x$ , and the above-mentioned nucleation barrier, two counterpropagative kinks are created. This is at the origin of the back-fire instability, as will be further discussed in Sec. V (see also Ref. 27).

#### V. AN EXPLANATION FOR THE BACK-FIRING INSTABILITY

In order to give a simple description, we restrict ourselves to studying Eq. (1) in the reference frame of a stable propagating kink, with Neumann boundary conditions at the rear and Dirichlet boundary conditions at the front of the kink  $A=A_L$ . We shall investigate the codimension-two point,  $P$ , of the phase diagram of Fig. 2 where the three regions meet. In this parameter region, we look for the functional phase portraits, before and after the saddle-node bifurcation of the phase kinks. Each solution of system (1) has a stable and an unstable manifold, and one can try to understand the evolution by investigating the connections between these solutions via the manifolds. Accordingly, the spatiotemporal dynamics may then be assessed by following the flows in the phase portraits. The advantage of this approach is that the description is purely geometrical.

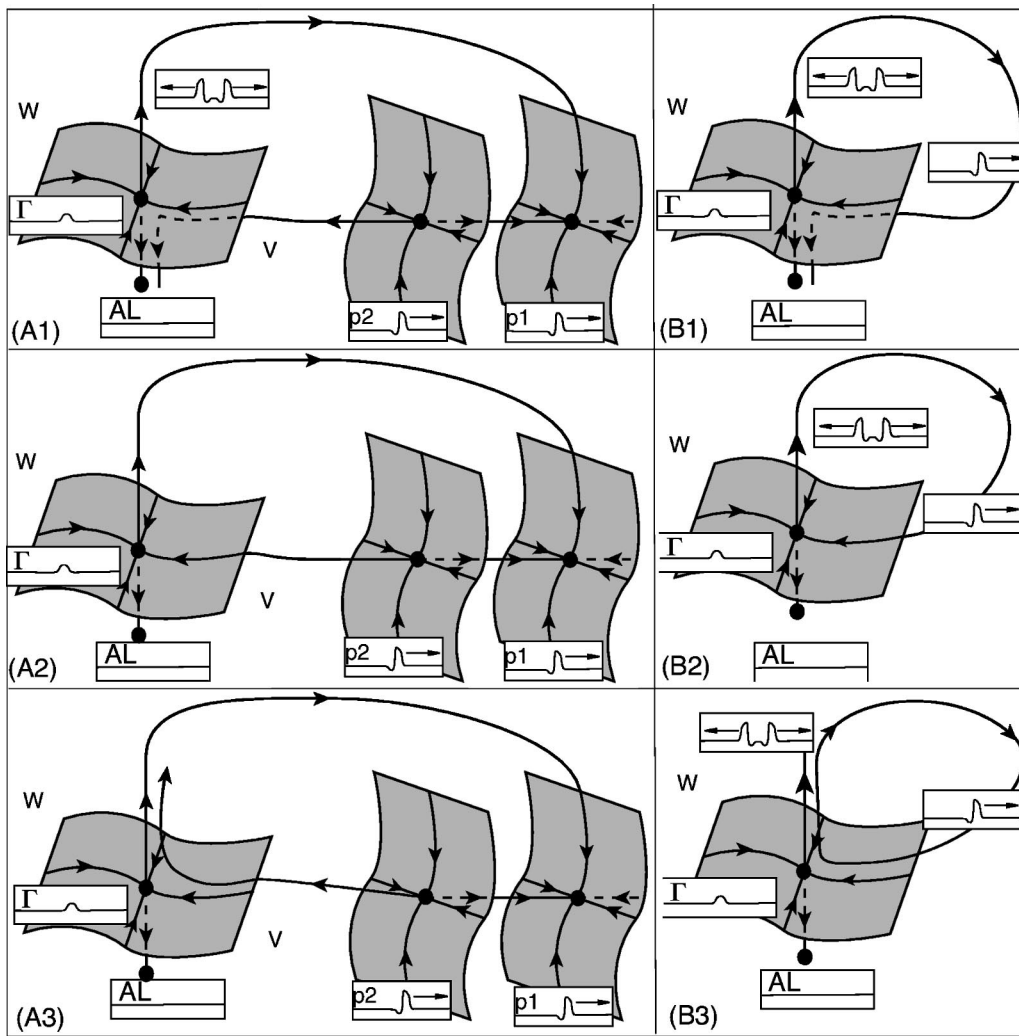


FIG. 4. Sketch of the functional phase portrait of Eq. (1). The black disks represent the solutions of the ODE, and the oriented black curves show how the flow is organized. In order to associate the spatiotemporal dynamics with the flow, we also show the profile of the complex field,  $A$ , along the flow. (A1) The unstable manifold,  $\mathcal{W}_u(\phi_+)$ , goes under the nucleation manifold,  $\mathcal{W}_s(\Gamma)$ . (A2) The unstable manifold,  $\mathcal{W}_u(\phi_+)$ , goes into the nucleation manifold,  $\mathcal{W}_s(\Gamma)$ . (A3) The unstable manifold,  $\mathcal{W}_u(\phi_+)$ , goes over the nucleation manifold,  $\mathcal{W}_s(\Gamma)$ . (B1) The unstable manifold,  $\mathcal{W}_u(\phi_+)$ , goes under the nucleation manifold. After the saddle-node bifurcation, the only attractor is the homogeneous stable solution. (B2) The unstable manifold,  $\mathcal{W}_u(\phi_+)$ , goes into the nucleation manifold, thus at the bifurcation point, a homoclinic loop is formed. (B3) The unstable manifold,  $\mathcal{W}_u(\phi_+)$ , goes over the nucleation manifold, and a quasi-homoclinic loop remains.

We first focus our study in the parameter regime before the saddle-node bifurcation where we know that the functional phase portrait has four fixed points: the two kinks,  $\phi_{+,-}$ , the nucleation solution,  $\Gamma$ , and the spatially homogeneous solution,  $A_L$ . Due to the saddle-node bifurcation, we also know that  $\phi_+$  has an unstable manifold,  $\mathcal{W}_u(\phi_+)$ , of dimension one, since the eigen-spectrum of  $\phi_+$  has only one real positive eigenvalue. Thus, the heteroclinic connection between  $\phi_+$  and  $\Gamma$  has codimension one. Hence, we expect three different cases, depending on the location of the unstable manifold,  $\mathcal{W}_u(\phi_+)$ , of  $\phi_+$ , relative to the stable manifold of  $\Gamma$ ,  $\mathcal{W}_s(\Gamma)$  (Fig. 4). The three options are: (A1) the unstable manifold,  $\mathcal{W}_u(\phi_+)$ , goes under the nucleation manifold,  $\mathcal{W}_s(\Gamma)$ , as seen in Fig. 4(A1); (A2) the unstable manifold,  $\mathcal{W}_u(\phi_+)$ , goes into  $\mathcal{W}_s(\Gamma)$  as pictured in Fig. 4(A2); (A3) the unstable manifold,  $\mathcal{W}_u(\phi_+)$ , goes over  $\mathcal{W}_s(\Gamma)$  as shown in Fig. 4(A3).

When the saddle-node bifurcation occurs, the two fixed

points,  $\phi_+$  and  $\phi_-$ , coalesce. Thus depending on the location of the unstable manifold,  $\mathcal{W}_u(\phi_+)$ , with respect to the nucleation manifold,  $\mathcal{W}_s(\Gamma)$ , prior to this bifurcation, we obtain three new cases: (B1) the only attractor is the rest state,  $A = A_L$ , as seen in Fig. 4(B1); (B2) the phase portrait exhibits a homoclinic connection with the nucleation solution, as pictured in Fig. 4(B2); (B3) a limit cycle is formed, related to a nearly homoclinic periodic solution, as shown in Fig. 4(B3).

In the case (B3), the flow of the limit cycle passes in the region where the phase kink exists. As a consequence, one sees in the numerical simulation of Eq. (1) a propagating phase kink-like structure (phase kinks are no longer solutions). After a finite time interval,  $\tau$ , the flow goes away from this region and the kink is destroyed. Then the flow passes near the nucleation solution,  $\Gamma$ , where it stays during another finite time interval,  $T$ . This is the nucleation process. Then the flow escapes from this region and two counterpropagat-

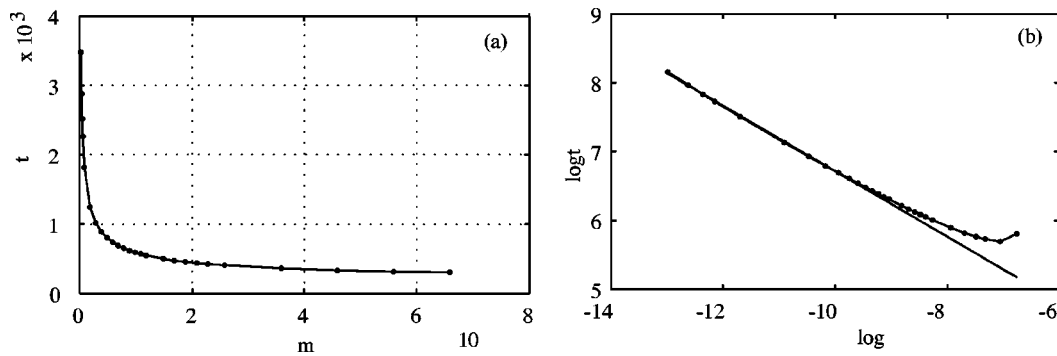


FIG. 5. (a) Divergence of the period,  $\tau$ , for the transition from I to III vs  $\mu = B - B_0$ . (b) Log-log plot of the period vs distance to the threshold. Parameter values:  $B_0 \approx 0.034\ 741\ 7$ ,  $\alpha = 1$ ,  $\nu = 1.044$ , and  $\beta = 0$ .

ing kinks are created. The flow goes back subsequently to the phase kink region, as one phase kink is destroyed at the left boundary. Since this process occurs periodically one sees a periodic behavior. If the time  $T$  is small, the pseudo-phase kink propagates with an almost constant velocity and periodically with a period  $\tau$  “back-fires” a new kink behind it.

The transition between evolutions I and II is related to the saddle-node bifurcation of the phase kinks described in the previous sections [i.e., transition between (A1) and (B1)]. The transition line observed in the simulation (Fig. 2), corresponds exactly to the bifurcation line  $B = B_{SN}(\nu, \alpha)$  that has been computed with the continuation software AUTO.

The transition between cases I and III is also related to the saddle-node bifurcation of pulses. When the phase portrait changes from (A3) to (B3), a closed loop is formed, and a limit cycle is created. The birth of a limit cycle due to a saddle-node bifurcation is an Andronov saddle-node bifurcation.<sup>29</sup> The typical feature of this bifurcation is the appearance of a limit cycle with a period that diverges at threshold as  $\tau \approx \mu^{-1/2}$ , where  $\mu$  is the distance from the bifurcation line.<sup>29</sup> The characteristic divergence of the period has been captured numerically and shown in Fig. 5.

It remains to explain the transition from type II to type III that leads to the topological change of the phase portrait from (B1) to (B3). Since a homoclinic loop is formed [Fig. 4(B2)], this transition is an Andronov homoclinic bifurcation.<sup>29</sup> A nearly homoclinic limit cycle [Fig. 4(B3)] appears with a period that diverges at threshold as  $T = (1/\lambda)\log(1/\epsilon)$ , where  $\epsilon$  is the distance to the bifurcation,

and  $\lambda$  is the unstable eigenvalue of the saddle point to which the homoclinic cycle tends to. In our context, the saddle point is the nucleation solution,  $\Gamma$ ,<sup>29</sup> and  $\lambda$  is the real positive eigenvalue that belongs to its spectrum. To substantiate our claim, the period of the limit cycle has been obtained by integrating numerically Eq. (1) and the logarithmic behavior of  $T$  is presented in Fig. 6. From the numerical data, we can evaluate the prefactor of the divergence. It is  $\lambda = 0.0278 \pm 5 \times 10^{-4}$ . The eigenvalue  $\lambda$  has also been obtained by numerical computation of the eigenspectrum of the nucleation solution  $\Gamma(x)$ . We found  $\lambda = 0.0275 \pm 8 \times 10^{-4}$ . These two completely independent findings are in agreement and confirm the existence of the homoclinic bifurcation.

Let us now consider the back-firing phenomenon when many pulses propagate. If the phase kinks are well separated, then each phase kink does not feel the presence of its neighbors. Indeed, the propagating pulses have tails that tend exponentially fast to the stable rest state,  $A_L$ . As a consequence, the scenario depicted for one pulse in this section may then be applied for each pulse present in the field  $A$ . Hence in the back-firing regime, each pulse has a finite lifetime proportional to  $\tau$  and the time necessary for creating counterpropagating pulses is related to  $T$ .

For illustration, we have plotted the spatiotemporal recordings of the field  $A$  in two limit cases. In Fig. 7(a), near the saddle-node bifurcation, the back-firing period is dominated by the time,  $\tau$ , associated to the saddle-node bifurcation. The nearly homoclinic cycle evolution is presented in

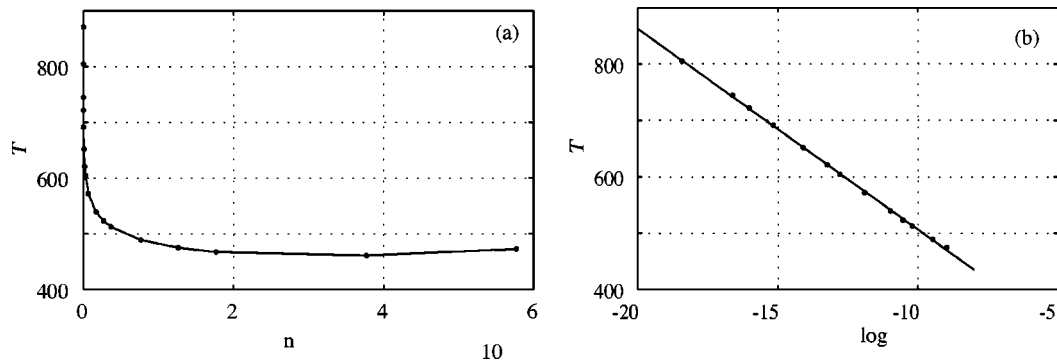


FIG. 6. (a) Divergence of the period of phase kink for the transition from II to III vs  $\epsilon = \nu_h - \nu$ . (b) Semi-log plot of the period vs distance to the threshold. Parameter values:  $B = 0.034\ 746$ ,  $\alpha = 1$ ,  $\nu_h = 1.042\ 423\ 24$ , and  $\beta = 0$ .

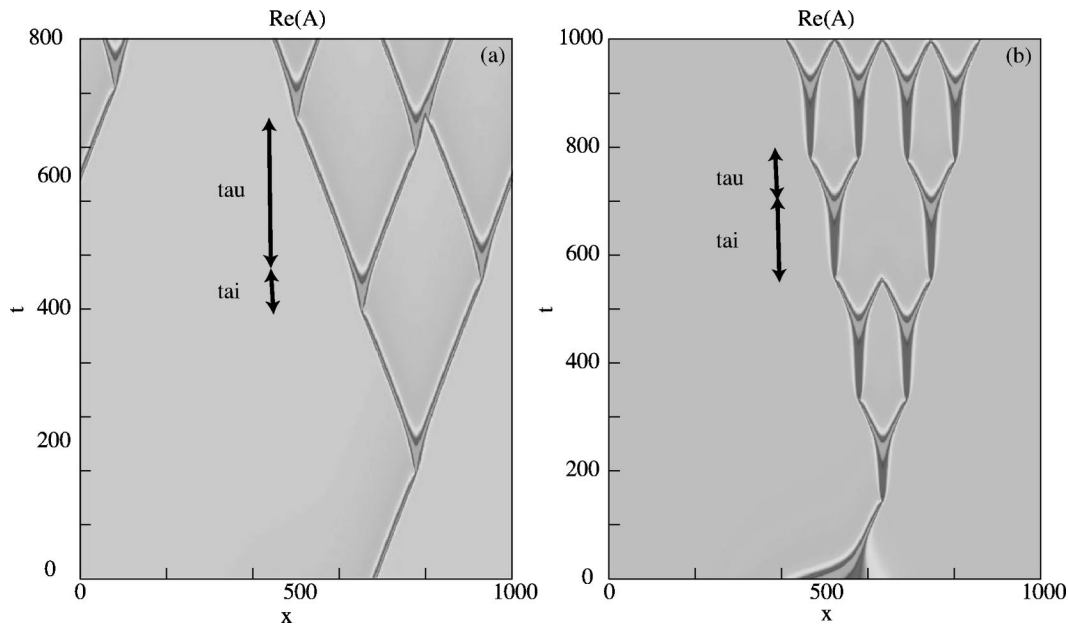


FIG. 7. Spatiotemporal diagrams of the back-firing regime near transitions. (a) Near the homoclinic bifurcation corresponding to a change in the phase portrait from (B1) to (B3); parameter values:  $\alpha=1$ ,  $\beta=0$ ,  $\nu=1.05$ , and  $B=0.37$ . (b) Near the saddle-node bifurcation of the pulses corresponding to a change in the phase portrait from (A3) to (B3); parameters are the same as (a) but with  $B=0.04$ .

Fig. 7(b), where the time lapse spent near the nucleation solution is made explicit.

## VI. A POSSIBLE MECHANISM FOR SPATIOTEMPORAL INTERMITTENCY AND CONCLUSIONS

Since the scenario discussed in the preceding sections is geometric, we expect to offer a robust description with universality. The first necessary condition for obtaining the back-firing instability is the saddle-node bifurcations of pulses. This feature has already been noted in model chemical systems,<sup>10,30</sup> and in the CGLE.<sup>2,3</sup> The second necessary condition is an heteroclinic connection between the stable manifold of the nucleation solution and the unstable manifold of the unstable pulse.

The unfolding of the bifurcation point,  $P$ , has been done following the phase kink in its moving frame. As a consequence, we underestimated the influence of the neighboring pulses. The interaction at a given time is expected to be small due to the exponentially fast convergence of the phase kink toward the stable state,  $A_L$ . Note that we earlier assumed that a collision of two counterpropagative kinks leads to their annihilation. In fact it appears that at  $(t,x) \sim (800,700)$  [Fig. 7(a)], a phase kink collides (call it R) with a newly created phase kink (call it L) which survives after the collision. Close inspection of the collision process shows that the kink, L, had not been properly formed, and hence the collision occurs during the nucleation process. The kink, R, just contributed to overcome the nucleation manifold.

The other kind of interaction that we consider to be important in the evolution is the following memory effect. In the study of the bifurcation scenario, we have assumed that the kink propagates in a clean, homogeneous medium where  $A=A_L$ . In fact, this hypothesis may be open to discussion. When the rest state,  $A=A_L$ , is perturbed locally albeit

slightly, there is a characteristic relaxation time that may be quite long since we are in the neighborhood of the Arnold tongue boundary,  $B=B_T(\nu, \alpha)$ . Accordingly, when a pulse propagates, it leaves behind a medium that has not completely relaxed to  $A=A_L$ . This memory effect can be seen, for example in Fig. 1 at  $(t,x) \sim (200,200)$ . There are smooth gray regions left behind by dying pulses that influence the subsequent back-firing process at  $(t,x) \sim (220,200)$ . The nucleation process involves a very precise threshold and when one kink undergoes back-firing, the nucleation threshold may be changed due to the history of the medium. In our analysis, the nucleation manifold is associated to a saddle point, the nucleation solution  $\Gamma$ . For each back-firing process of each of the phase kinks present in the medium, the nucleation manifold selects whether or not a new kink is going to be emitted. This feature, already noticed in Ref. 27, is exponentially amplified. It is the reason why for asymptotic long time intervals (like in Fig. 1), very complex patterns are observed.

## ACKNOWLEDGMENTS

The authors wish to thank P. Coulet, M. Clerc, A. S. Mikhailov, and A. Pikovsky for fruitful discussions. This work has been supported by the Spanish Ministry of "Educacion y Cultura" (Grant No. PB96-599), by the European Union (TMR Grant No. FMRX-CT96-0010), and by CONICYT (Fondecyt Grant). Part of the numerical simulations has been performed using the NLKit software developed at Institut Non-Linéaire de Nice, France.

<sup>1</sup>I. S. Aranson and L. Kramer, Rev. Mod. Phys. **74**, 99 (2002).

<sup>2</sup>L. Brusch, M. Zimmermann, M. van Hecke, M. Bär, and A. Torcini, Phys. Rev. Lett. **85**, 86 (2000).

- <sup>3</sup>L. Bruschi, A. Torcini, M. van Hecke, M. G. Zimmermann, and M. Bär, *Physica D* **160**, 127 (2001).
- <sup>4</sup>See, e.g., A. A. Nepomnyashchy, M. G. Velarde, and P. Colinet, *Interfacial Phenomena and Convection* (CRC-Chapman and Hall, Boca Raton, 2002), Chap. 7.
- <sup>5</sup>H. Chaté, A. S. Pikovsky, and O. Rudzick, *Physica D* **131**, 17 (1999).
- <sup>6</sup>M. Bär, M. Hildebrand, M. Eiswirth, M. Falcke, H. Engel, and M. Neufeld, *Chaos* **4**, 499 (1994).
- <sup>7</sup>Y. Hayase and T. Ohta, *Phys. Rev. Lett.* **81**, 1726 (1998).
- <sup>8</sup>H. Chaté and P. Manneville, *Phys. Rev. Lett.* **58**, 112 (1987).
- <sup>9</sup>M. van Hecke, *Phys. Rev. Lett.* **80**, 1896 (1998).
- <sup>10</sup>M. G. Zimmermann, S. O. Firlé, M. A. Natiello, M. Hildebrand, M. Eiswirth, M. Bär, A. K. Bangia, and I. G. Kevrekidis, *Physica D* **110**, 92 (1997).
- <sup>11</sup>V. Petrov, S. K. Scott, and K. Showalter, *Philos. Trans. R. Soc. London, Ser. A* **347**, 631 (1994).
- <sup>12</sup>L. A. Lugiato, L. M. Narducci, D. K. Bandy, and C. A. Pennise, *Opt. Commun.* **46**, 64 (1983); see also H. G. Solari and G. L. Oppo, *ibid.* **111**, 173 (1994).
- <sup>13</sup>H. Meinhardt, *The Algorithmic Beauty of Seashells* (Springer, Berlin, 1995).
- <sup>14</sup>J. Keener and J. Sneyd, *Mathematical Physiology* (Springer, Berlin, 1998).
- <sup>15</sup>C. Morris and H. Lecar, *Biophys. J.* **35**, 193 (1981).
- <sup>16</sup>D. P. Vallette, G. Jacobs, and J. P. Gollub, *Phys. Rev. E* **55**, 4274 (1997).
- <sup>17</sup>J. M. Gambaudo, *J. Diff. Eqns.* **57**, 172 (1985).
- <sup>18</sup>P. Couillet and K. Emilsson, *Physica D* **61**, 119 (1992); see also *Physica A* **188**, 190 (1992).
- <sup>19</sup>S. Rasband, *Chaotic Dynamics of Nonlinear Systems* (Wiley, New York, 1990), pp. 130 and 131.
- <sup>20</sup>O. Rudzick, Ph.D. thesis, Universität Potsdam, 1998.
- <sup>21</sup>M. C. Cross and P. C. Hohenberg, *Rev. Mod. Phys.* **65**, 851 (1993).
- <sup>22</sup>E. J. Doedel, H. B. Keller, and J. P. Kernévez, *Int. J. Bifurcation Chaos Appl. Sci. Eng.* **1**, 493 (1991); **1**, 745 (1991).
- <sup>23</sup>Y. Pomeau, *Physica D* **23**, 1 (1986).
- <sup>24</sup>M. Argentina, P. Couillet, and L. Mahadevan, *Phys. Rev. Lett.* **79**, 2803 (1997).
- <sup>25</sup>M. Argentina, P. Couillet, and V. Krinsky, *J. Theor. Biol.* **205**, 47 (2000).
- <sup>26</sup>Y. Nishiura, T. Teramoto, and K. Ueda, *Chaos* **13**, 962 (2003).
- <sup>27</sup>M. van Hecke and M. Howard, *Phys. Rev. Lett.* **86**, 2018 (2001).
- <sup>28</sup>Y. Kuramoto, *Chemical Oscillations, Waves and Turbulence* (Springer, Berlin, 1984).
- <sup>29</sup>A. A. Andronov, E. A. Leontovich, I. I. Gordon, and A. G. Maier, *Theory of Bifurcation of Dynamical Systems on the Plane* (Wiley, New York, 1971).
- <sup>30</sup>M. Or-Guil, J. Krishnan, I. G. Kevrekidis, and M. Bär, *Phys. Rev. E* **64**, 046212 (2001).